

Field-induced quadrupolar quantum criticality in $\text{PrV}_2\text{Al}_{20}$

Yasuyuki Shimura,^{1,*} Masaki Tsujimoto,¹ Bin Zeng,² Luis Balicas,² Akito Sakai,^{1,3} and Satoru Nakatsuji^{1,4,†}

¹*Institute for Solid State Physics, The University of Tokyo, Kashiwa, Chiba 277-8581, Japan*

²*National High Magnetic Field Laboratory (NHMFL), Florida State University, Tallahassee, Florida 32310, USA*

³*I. Physikalisches Institut, Georg-August-Universität Göttingen, 37077 Göttingen, Germany*

⁴*PRESTO, Japan Science and Technology Agency (JST), 4-1-8 Honcho Kawaguchi, Saitama 332-0012, Japan*

(Received 29 November 2014; revised manuscript received 5 May 2015; published 4 June 2015)

$\text{PrV}_2\text{Al}_{20}$ is a heavy-fermion superconductor based on the cubic Γ_3 doublet that exhibits nonmagnetic quadrupolar ordering below ~ 0.6 K. Our magnetotransport study on $\text{PrV}_2\text{Al}_{20}$ reveals field-induced quadrupolar quantum criticality at $\mu_0 H_c \sim 11$ T applied along the [111] direction. Near the critical field $\mu_0 H_c$ required to suppress the quadrupolar state, we find a marked enhancement of the resistivity $\rho(H, T)$, a divergent quasiparticle effective mass and concomitant non-Fermi-liquid (NFL) behavior [i.e., $\rho(T) \propto T^n$ with $n \leq 0.5$]. We also observe the Shubnikov-de Haas effect above $\mu_0 H_c$, indicating effective mass enhancement or $m^*/m_0 \sim 10$. This reveals the competition between the nonmagnetic Kondo effect and the intersite quadrupolar coupling which leads to pronounced NFL behavior in an extensive region of T and $\mu_0 H$ emerging from the quantum-critical point.

DOI: [10.1103/PhysRevB.91.241102](https://doi.org/10.1103/PhysRevB.91.241102)

PACS number(s): 75.47.-m, 72.15.Qm, 75.25.Dk

Quantum criticality in correlated electron systems has attracted significant attention because of the formation of novel quantum phases such as exotic superconductivity in the vicinity of a quantum-critical point (QCP) [1]. Moreover, the breakdown of the standard Fermi-liquid behavior has been seen almost routinely nearby a magnetic QCP in a variety of strongly correlated electron systems, ranging from cuprates and iron pnictides to heavy-fermion intermetallics [2,3]. Whether another type of instability such as orbital ordering and its associated orbital fluctuations may drive novel types of metallic states and unconventional superconductivity has been an active area of research [1,4–8]. Experimentally, however, quantum criticality due solely to an orbital origin was never observed in metallic systems.

For the study of quantum criticality, $4f$ -electron systems are well suited. These systems provide various archetypical examples due to the availability of high-purity single crystals and the relatively low characteristic energy scales, which are highly tunable by disorder-free control parameters such as magnetic field or pressure. To date, among heavy-fermion intermetallics, most of the study on QC has been performed on compounds containing either Ce ($4f^1$) or Yb ($4f^{13}$) (see, for example, Refs. [9–13]) ions whose crystalline-electric-field (CEF) ground state is composed of Kramers doublets and therefore is magnetic.

In transition-metal systems, the coupling between spins and orbitals is unavoidable and produces various interesting spin-orbital ordered and disordered states [14,15]. In contrast, an f -electron system may provide a nonmagnetic CEF ground-state doublet, where orbitals are the only active degree of freedom. In effect, some Pr ($4f^2$)-based cubic compounds are found to host the Γ_3 non-Kramers ground-state doublet, which has no magnetic moment but carries an electric quadrupole moment. In these systems, due to strong intra-atomic spin-orbit coupling, the total angular momentum J represents the

magnetic and orbital states and, in particular, the electric quadrupole moment corresponds to the orbital degree of freedom. A number of cubic $4f^2 \Gamma_3$ systems were studied and various interesting electric phenomena were experimentally reported including a ferro- and antiferroquadrupolar ordering depending on the type of the Ruderman-Kittel-Kasuya-Yosida (RKKY)-type interaction [16–20]. As a competing effect, a nonmagnetic form of the Kondo effect is proposed that quenches the quadrupole moments [21,22]. Thus, the tuning of these competing effects may lead to quadrupolar QCP.

In fact, quadrupolar quantum criticality was suggested by recent experiments on the new cubic Γ_3 systems $\text{PrT}_2\text{Al}_{20}$, where T corresponds to a transition metal such as Ti or V [23–26]. In these systems, the hybridization between the f moments and the conduction (c -) electrons is found to be not only strong but tunable. The strong c - f hybridization is evident from a number of observations, including the Kondo effect in the resistivity [i.e., $\rho(T) \propto -\ln T$] [23], a Kondo-resonance peak observed near the Fermi energy [27], and a large hyperfine constant in the nuclear magnetic resonance (NMR) measurements [28]. The tunability of the hybridization strength in $\text{PrT}_2\text{Al}_{20}$ is demonstrated by both chemical and physical pressure measurements: the substitution of Ti by V enhances the Kondo effect and induces an anomalous metallic behavior due to the hybridization. $\text{PrTi}_2\text{Al}_{20}$ exhibits a ferroquadrupole ordering at $T_Q = 2$ K with a subsequent superconducting (SC) transition at $T_c = 0.2$ K [23,24]. While the SC effective mass of $\text{PrTi}_2\text{Al}_{20}$ is moderately enhanced under ambient pressure, i.e., $m^*/m_0 \sim 16$ (m_0 is the free electron mass), the application of pressure increases T_c up to 1 K and m^*/m_0 up to 110 at $P \sim 8$ GPa, while suppressing T_Q [25]. This indicates that the pressure-induced heavy-fermion superconductivity emerges in the vicinity of a putative quadrupolar QCP.

Evidence for strong hybridization in $\text{PrV}_2\text{Al}_{20}$ is further provided by the recent discovery of heavy-fermion superconductivity at $T_c = 50$ mK with a large specific-heat jump $\Delta C/T \sim 0.3$ J/mol K² below $T_Q = 0.6$ – 0.7 K under ambient pressure [26]. The effective mass of the quasiparticles participating in the superconducting condensate is found to be as large as $140m_0$, which is one order of magnitude larger than

*simu@issp.u-tokyo.ac.jp

†satoru@issp.u-tokyo.ac.jp

that of its Ti analog [24]. This result indicates that $\text{PrV}_2\text{Al}_{20}$ should be located in the vicinity of a QCP associated *only* with multipole moments.

To realize such quantum criticality due to multipole moments, the magnetic field is another useful control parameter that couples quadratically with quadrupole moments, thus more weakly than with magnetic moments. The high-field phase diagram of $\text{PrV}_2\text{Al}_{20}$ was investigated through specific-heat measurements under fields up to 9 T applied along all three main crystallographic orientations. Overall, the low-field phase boundaries for the [100], [110], and [111] directions are very similar to one another and nearly independent of $\mu_0 H$, as often observed in various quadrupolar ordered systems [20,23]. Moreover, high-field magnetization measurements revealed a field-induced first-order transition at $\mu_0 H \sim 11$ T for $H \parallel [100]$, which is most likely due to the switching of the quadrupole order parameter in the Γ_3 ground doublet [29].

Here, we report the discovery of field-tuned quantum criticality based solely on the quadrupolar (orbital) degrees of freedom at ambient pressure in $\text{PrV}_2\text{Al}_{20}$. We studied, through magnetotransport measurements, the magnetic phase diagram of $\text{PrV}_2\text{Al}_{20}$ for $H \parallel [111]$. We found unusual non-Fermi-liquid behavior, i.e., $\rho = \rho_0 + AT^n$ with $n \leq 0.5$, a divergent quasiparticle effective mass, and a large enhancement in the residual resistivity ρ_0 around the magnetic field-induced quantum-phase transition at the critical field $\mu_0 H_c \sim 11$ T, where the quadrupolar transition temperature is suppressed to absolute zero. In addition, our observation of quantum oscillations revealed a heavy mass state with $m^*/m_0 > 10$ in the paraquadrupolar state beyond $\mu_0 H_c$, indicating a nonmagnetic Kondo effect competing with the quadrupolar coupling as the origin of the pronounced quantum criticality observed over an extensive region of T and $\mu_0 H$. The experimental condition is described in detail in the Supplemental Material [30].

The temperature dependence of the resistivity $\rho(T)$ in both the low-field ($\mu_0 H \leq 8$ T) and the high-field ($\mu_0 H \geq 9.5$ T) regions is presented in Figs. 1(a) and 1(b), respectively. Both the magnetic field and the electric currents were applied along the [111] direction. When the field is lower than 10 T, one observes a sudden decrease in $\rho(T)$ upon cooling due to the quadrupolar phase transition. Correspondingly, a peak is observed in the T derivative of the resistivity at a low temperature T_Q which systematically changes with field, as shown in Fig. 1(c). On the other hand, the resistivity under fields surpassing 11 T shows such a smooth temperature dependence that the anomaly associated with the quadrupolar ordering no longer exists. Thus, a quantum-phase transition between the low-field quadrupolar and high-field paraquadrupolar phases should be located at $\mu_0 H_c \sim 11$ T. Such a field-induced suppression of a quadrupolar phase was predicted for the $\text{PrT}_2\text{Al}_{20}$ system using a mean-field theory based on a localized picture [31]. Previous magnetization measurements [29] for fields aligned along the [111] direction did not detect evidence for an ordered state, in contrast to what is observed for fields aligned along the [100] direction. This is consistent with our results.

Under a field of 11 T, the resistivity displays a sublinear dependence on T , which contrasts markedly with the Fermi-liquid behavior, i.e., $\rho \propto T^2$, shown in the inset of Fig. 1(b).

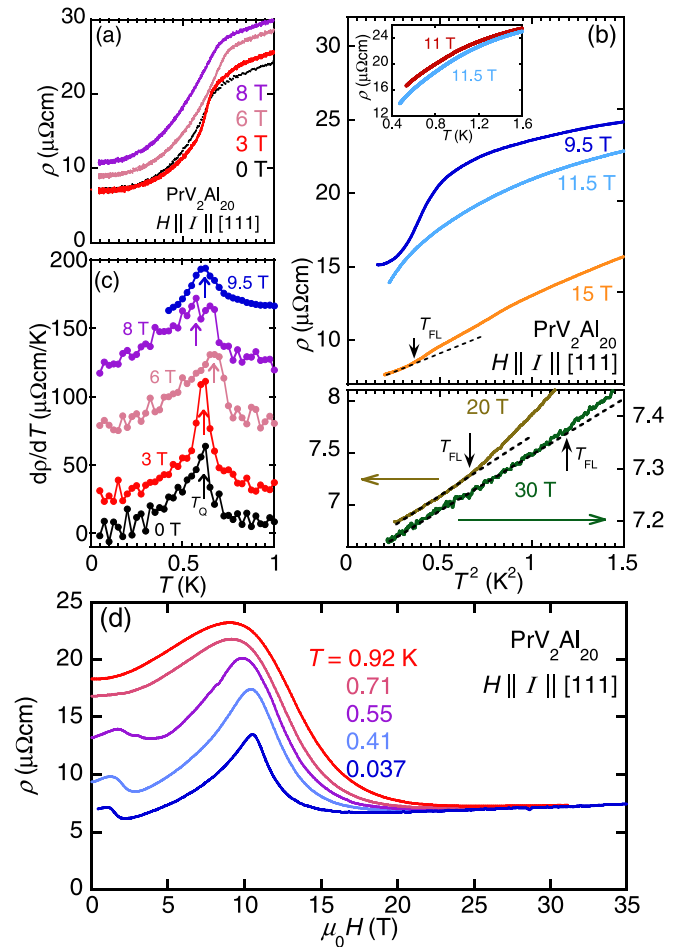


FIG. 1. (Color online) (a),(b) Longitudinal resistivity ρ for $\text{PrV}_2\text{Al}_{20}$ single crystals as a function of temperature T under magnetic fields. The solid arrow indicates the characteristic temperature T_{FL} below which $\rho(T)$ exhibits a T^2 dependence (dashed line). (c) Derivative of the resistivity with respect to temperature $d\rho/dT$ and as a function of T , for fields below 10 T. The data points are vertically shifted for clarity. The arrows indicate the quadrupolar transition temperature T_Q . (d) ρ as a function of $\mu_0 H \parallel [111]$ at various temperatures.

In contrast, for fields beyond 15 T, the resistivity displays a superlinear or T^2 dependence at the lowest temperatures, as seen in Fig. 1(b). A detailed analysis of the field and temperature dependence of ρ will be described below. Figure 1(d) displays the field dependence of the magnetoresistivity for $T < 1$ K. $\rho(H)$ exhibits a sharp peak at $\mu_0 H_c \sim 11$ T. In addition, below 10 T, it displays a marked drop as the temperature is reduced below $T = 0.6$ K, due to the transition towards a quadrupolar ordered state. If this peak resulted solely from thermal critical fluctuations associated with a finite temperature transition between the quadrupolar phase to the paraquadrupolar state, this peak would be expected to shift to lower fields with increasing T and eventually reach zero field near $T_Q \sim 0.6$ K. However, in $\text{PrV}_2\text{Al}_{20}$, a pronounced peak is still observed at nearly the same field ~ 11 T at $T \sim 1$ K $\gg T_Q$, indicating the development of quantum-critical scattering at $\sim \mu_0 H_c$ and at much higher T 's than T_Q . In addition to the main peak at

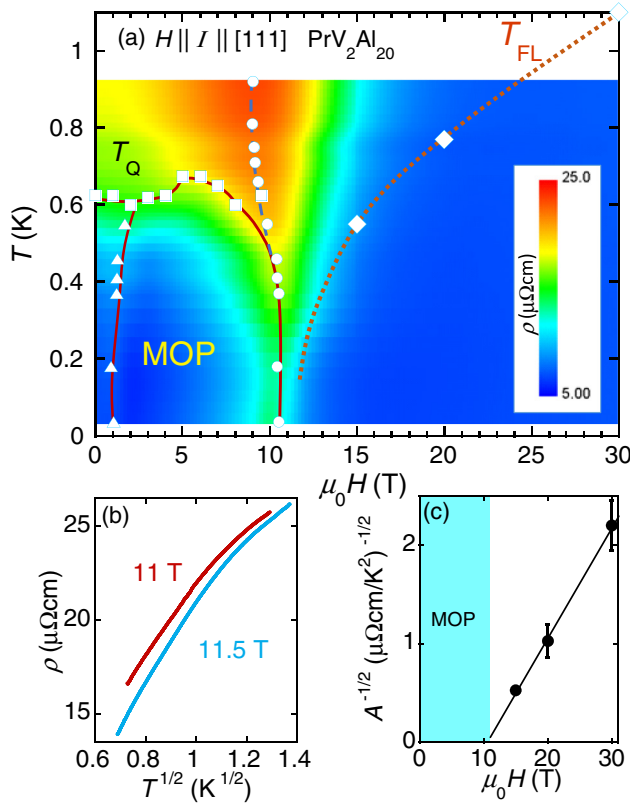


FIG. 2. (Color online) (a) Magnetic phase diagram of $\text{PrV}_2\text{Al}_{20}$ for fields, and current I , parallel to the $[111]$ direction. Color plot indicates the $\rho(T, H)$ values obtained from H scans under constant T . Circles indicate the peak position at $\mu_0 H_c \sim 11$ T, separating the low-field multipole ordering phase (MOP) and the paraquadrupolar state at high fields. Triangles represent small peaks observed in $\rho(H)$ for fields below 2 T. The solid line and broken line show the transition temperature/field of the multipole ordered phase and the peak position in $\rho(H)$, respectively. Squares and diamonds, respectively, indicate T_Q as determined from the peak in $d\rho(T)/dT$ and a characteristic temperature T_{FL} below which $\rho(T)$ follows the Fermi-liquid T^2 law. The dotted line is a guide to the eyes. (b) ρ as a function of $T^{1/2}$ under $\mu_0 H = 11$ and 11.5 T. (c) Field dependence of $A^{-1/2}$, where A is the T^2 coefficients in $\rho(T)$. The solid line is the fit to $\sqrt{A} = \sqrt{A_0}/(\mu_0 H - \mu_0 H_c)$.

~ 11 T, a small peak was observed below 2 T in the quadrupolar ordered state below 0.6 K. This may be associated with the change in the order parameters such as the lifting of the degeneracy between the O_0^2 and O_2^2 states [31].

To clearly illustrate the field-induced enhancement of the resistivity above T_Q , Fig. 2(a) shows a contour plot of ρ as a function of both T and $H \parallel [111]$. The change in color between blue and green at ~ 0.5 K found below 10 T follows the quadrupolar transition temperature T_Q (squares) determined by the temperature scans discussed above. This line of T_Q connects smoothly with the line depicting the peak position (circle) in the field dependence of the resistivity $\rho(H)$. These results indicate that the peak in the magnetoresistance at low temperatures corresponds to the quadrupolar phase boundary [solid line in Fig. 2(a)], which reaches the quantum-critical point at $\mu_0 H_c \sim 11$ T.

Remarkably, the peak observed in $\rho(H)$ around 11 T survives up to ~ 1 K $> T_Q$, as discussed above, and this pronounced peak in $\rho(T, H)$ [red region in Fig. 2(a)], which is observed in the paraquadrupolar regime, cannot be explained within a simple localized f -moment scenario. Figure 2(b) shows $\rho(T)$ as a function of $T^{1/2}$ at $\mu_0 H = 11$ T near the quantum-critical field. $\rho(T)$ under $\mu_0 H = 11$ and 11.5 T shows a concave curvature, indicating that the exponent n in $\rho(T) = \rho_0 + AT^n$ is even smaller than 0.5. On the contrary, above 15 T, $\rho(T)$ exhibits a convex curvature indicating the emergence of Fermi-liquid behavior at the lowest T s, as shown in Fig. 1(b). The characteristic temperature T_{FL} below which $\rho(T)$ displays FL behavior or $\rho(T) = \rho_0 + AT^2$ increases with field [Fig. 2(a)]. Figure 2(c) indicates the field dependence of $A^{-1/2}$ obtained from $\rho(T)$ above 15 T. Accordingly, upon approaching the quantum-critical field, the corresponding A values diverge, exceeding $\sim 5 \mu\Omega \text{cm}/\text{K}^2$. It can be fit to $\sqrt{A} = \sqrt{A_0}/(\mu_0 H - \mu_0 H_c^A)$ with $\sqrt{A_0} = 8.92 (\mu\Omega \text{cm T}/\text{K}^2)^{1/2}$, and $\mu_0 H_c^A = 10.5$ T [Fig. 2(c)]. Significantly, $\mu_0 H_c^A$ is found to be consistent with the critical field ~ 11 T determined by the peak in $\rho(H)$. According to the Kawasaki-Woods relation, the critical enhancement in $A^{1/2}$ indicates the divergence of the effective mass upon approaching the QCP.

The sharp magnetoresistance peak at $\mu_0 H_c \sim 11$ T, which is observed even above T_Q , indicates a significant role for hybridization effects in the quantum criticality. In effect, at a pressure-induced quantum-critical point, the enhancement in the residual resistivity has been reported and attributed to quantum-critical fluctuations [2]. In Pr-based compounds with a Γ_3 ground doublet, such an enhancement in ρ_0 was also observed under zero field, especially above ~ 7 GPa in $\text{PrTi}_2\text{Al}_{20}$, which is accompanied by the suppression of the quadrupole order [25]. T_c as well as the effective mass m^* also increase considerably above ~ 7 GPa, while T_Q starts to decrease, suggesting the proximity to a putative quantum-critical point [25]. In $\text{PrV}_2\text{Al}_{20}$, the similarly dramatic enhancement in both ρ_0 and in $m^* \sim A^{1/2}$ under magnetic field, coupled to the anomalous T dependence of the resistivity at the critical field $\mu_0 H_c \simeq 11$ T, provides firm experimental evidence for field-induced quantum criticality based on the strong hybridization between the conduction electrons and the nonmagnetic quadrupolar/orbital degrees of freedom in the Γ_3 ground doublet. As discussed above, the resistivity follows $\rho = \rho_0 + AT^n$, with $n \leq 0.5$ at $\mu_0 H_c$, in sharp contrast to $n = 1$ and 1.5, which are usually observed around a QCP in Ce/Yb-based heavy-fermion compounds with a ground Kramers doublet [9–13].

Finally, the high quality of our single crystals allows us to observe the Shubnikov–de Haas (SdH) effect above the critical field. Figure 3(a) illustrates a representative trace of the oscillatory signal superimposed into $\rho(H)$ (after subtraction of a polynomial fit) at $T = 70$ mK as a function of inverse field $1/\mu_0 H$, under fields aligned at an angle $\theta = 75^\circ$ away from the $[111]$ direction and beyond the critical value required to suppress the quadrupolar state. The corresponding fast Fourier-transform spectra is shown in Fig. 3(b) for two values of T , respectively, at 60 mK (dark blue trace) and 220 mK (clear blue trace). One detects two main small frequencies, $F_\alpha \sim 190$ and $F_\beta \sim 290$ T. Figure 3(b) also displays two other traces for H

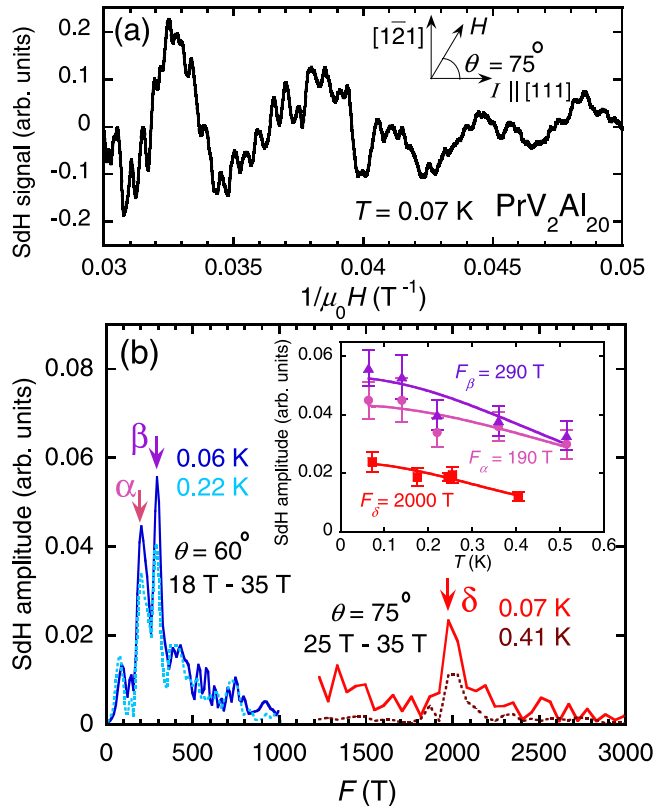


FIG. 3. (Color online) (a) Typical trace of the oscillatory signal due to the Shubnikov–de Haas effect (SdH), superimposed onto the $\rho(H)$ trace as a function of $\mu_0 H^{-1}$ for $T = 70$ mK and for an angle $\theta = 75^\circ$ from the [111] direction. (b) Fast Fourier transform (FFT) of the oscillatory signal for $\theta = 60^\circ$ and at $T = 60$ and 220 mK, respectively. One observes two prominent peaks at $F_\alpha \sim 190$ and $F_\beta \sim 290$ T. The same figure shows the FFT spectra for $\theta = 75^\circ$ and $T = 70$ and 410 mK. For this orientation, one detects a higher frequency $F_\delta \sim 2$ kT. Inset: Lifshitz-Kosevich fits of the SdH amplitude as a function of T from which we extract the corresponding effective masses m^* .

at an angle $\theta = 75^\circ$, and at $T = 70$ mK (dark orange trace) and 410 mK (brown trace), respectively, revealing a higher frequency $F_\delta \sim 2$ kT.

An important piece of information is provided by the inset in Fig. 3(b), which displays the amplitude of the FFT peaks as a function of T : solid lines are fits to the Lifshitz-Kosevich thermal damping term, i.e., $X/\sinh X$ with $X = 4\pi^3 k_B m^* T / eH$ (where k_B is the Boltzmann constant and e is the electron charge) from which we

extract the effective mass m^* for each F . The resulting mass values are $m_\alpha^* = (5.7 \pm 1.2)m_0$, $m_\beta^* = (6.8 \pm 1.2)m_0$, and $m_\delta^* = (10.6 \pm 1.2)m_0$, which are still moderately heavy, indicating the presence of the nonmagnetic Kondo effect based on the c - f hybridization. This indicates that the nonmagnetic Kondo effect has a much higher energy scale than the CEF gap at the critical field [30]. Thus, the quantum-critical behavior unveiled here cannot be ascribed to an f -electron localization transition involving the suppression of the Kondo effect at low fields. The charge carriers are so heavy as $m^* \sim 140m_0$ at zero field, and still display moderately heavy masses at high fields. de Haas–van Alphen (dHvA) measurements were performed also in the isostructural compound $\text{PrTi}_2\text{Al}_{20}$ which displays ferroquadrupole ordering below 2 K [32]. The effective masses extracted for the various Fermi-surface sheets range between 0.52 and 0.82 m^*/m_0 . These values are considerably smaller than the masses, ranging from 5.7 to 10 m^*/m_0 , observed in $\text{PrV}_2\text{Al}_{20}$. This difference in effective masses is qualitatively consistent with much heavier masses for $\text{PrV}_2\text{Al}_{20}$, or $\sim 140m_0$, versus $\sim 16m_0$ for $\text{PrTi}_2\text{Al}_{20}$ as estimated from their superconducting transition under zero field. In contrast with the divergence found in the A coefficient as $\mu_0 H \rightarrow \mu_0 H_c$, we could not detect any evolution of the cyclotron masses upon approaching the QCP, thus indicating that other, probably undetected, Fermi-surface sheets are involved in the QC phenomenology displayed by $\text{PrV}_2\text{Al}_{20}$, and that the detected cyclotronic orbits remain oblivious to the quantum fluctuations associated with orbital degrees of freedom. The observation of the SdH signal paves the path to further clarifying its electronic structure and to understanding the strong screening effects leading to the quadrupolar quantum criticality involving the prominent non-Fermi-liquid behavior observed in $\text{PrV}_2\text{Al}_{20}$.

We thank Y. Matsumoto, T. Tomita, T. Sakakibara, K. Araki, Y. Uwatoko, K. Matsubayashi, J. Suzuki, K. Miyake, K. Hattori, and H. Kusunose for useful discussions. This work was partially supported by Grants-in-Aid (No. 25707030 and No. 25887015) from JSPS, and by PRESTO, JST, Japan, and by the Program for Advancing Strategic International Networks to Accelerate the Circulation of Talented Researchers (Grant No. R2604) from the Japanese Society for the Promotion of Science R2604. Y.S. is partially supported by ICAM. The NHMFL is supported by NSF through Grant No. NSF-DMR-0084173 and the State of Florida. L.B. is supported by the US DOE-BES through Award No. DE-SC0002613. This work was supported in part by NSF Grant No. PHYS-1066293 and we acknowledge the hospitality of the Aspen Center for Physics.

- [1] P. Monthoux, D. Pines, and G. G. Lonzarich, *Nature (London)* **450**, 1177 (2007).
- [2] H. V. Löhneysen, A. Rosch, M. Vojta, and P. Wölfle, *Rev. Mod. Phys.* **79**, 1015 (2007).
- [3] P. Gegenwart, Q. Si, and F. Steglich, *Nat. Phys.* **4**, 186 (2008).

- [4] E. D. Bauer, N. A. Frederick, P.-C. Ho, V. S. Zapf, and M. B. Maple, *Phys. Rev. B* **65**, 100506 (2002).
- [5] K. Miyake, H. Kohno, and H. Harima, *J. Phys.: Condens. Matter* **15**, L275 (2003).
- [6] K. Hattori, *J. Phys. Soc. Jpn.* **79**, 114717 (2010).
- [7] H. Kontani and S. Onari, *Phys. Rev. Lett.* **104**, 157001 (2010).

- [8] Y. Yanagi, Y. Yamakawa, N. Adachi, and Y. Ono, *J. Phys. Soc. Jpn.* **79**, 123707 (2010).
- [9] N. D. Mathur, F. M. Grosche, S. R. Julian, I. R. Walker, D. M. Freye, R. K. W. Haselwimmer, and G. G. Lonzarich, *Nature (London)* **394**, 39 (1998).
- [10] H. Hegger, C. Petrovic, E. G. Moshopoulou, M. F. Hundley, J. L. Sarrao, Z. Fisk, and J. D. Thompson, *Phys. Rev. Lett.* **84**, 4986 (2000).
- [11] J. Paglione, M. A. Tanatar, D. G. Hawthorn, E. Boaknin, R. W. Hill, F. Ronning, M. Sutherland, L. Taillefer, C. Petrovic, and P. C. Canfield, *Phys. Rev. Lett.* **91**, 246405 (2003).
- [12] P. Gegenwart, J. Custers, C. Geibel, K. Neumaier, T. Tayama, K. Tenya, O. Trovarelli, and F. Steglich, *Phys. Rev. Lett.* **89**, 056402 (2002).
- [13] S. Nakatsuji, K. Kuga, Y. Machida, T. Tayama, T. Sakakibara, Y. Karaki, H. Ishimoto, S. Yonezawa, Y. Maeno, E. Pearson, G. G. Lonzarich, L. Balicas, H. Lee, and Z. Fisk, *Nat. Phys.* **4**, 603 (2008).
- [14] Y. Tokura and N. Nagaosa, *Science* **288**, 462 (2000).
- [15] S. Nakatsuji, K. Kuga, K. Kimura, R. Satake, N. Katayama, E. Nishibori, H. Sawa, R. Ishii, M. Hagiwara, F. Bridges, T. U. Ito, W. Higemoto, Y. Karaki, M. Halim, A. A. Nugroho, J. A. Rodriguez-Rivera, M. A. Green, and C. Broholm, *Science* **336**, 559 (2012).
- [16] P. Morin, D. Schmitt, and E. du Tremolet de Lacheisserie, *J. Magn. Magn. Mater.* **30**, 257 (1982).
- [17] H. Suzuki, M. Kasaya, T. Miyazaki, Y. Nemoto, and T. Goto, *J. Phys. Soc. Jpn.* **66**, 2566 (1997).
- [18] T. Onimaru, T. Sakakibara, N. Aso, H. Yoshizawa, H. S. Suzuki, and T. Takeuchi, *Phys. Rev. Lett.* **94**, 197201 (2005).
- [19] T. Onimaru, K. T. Matsumoto, Y. F. Inoue, K. Umeo, Y. Saiga, Y. Matsushita, R. Tamura, K. Nishimoto, I. Ishii, T. Suzuki, and T. Takabatake, *J. Phys. Soc. Jpn.* **79**, 033704 (2010).
- [20] T. Onimaru, K. T. Matsumoto, Y. F. Inoue, K. Umeo, T. Sakakibara, Y. Karaki, M. Kubota, and T. Takabatake, *Phys. Rev. Lett.* **106**, 177001 (2011).
- [21] D. L. Cox, *Phys. Rev. Lett.* **59**, 1240 (1987).
- [22] A. Yatskar, W. P. Beyermann, R. Movshovich, and P. C. Canfield, *Phys. Rev. Lett.* **77**, 3637 (1996).
- [23] A. Sakai and S. Nakatsuji, *J. Phys. Soc. Jpn.* **80**, 063701 (2011).
- [24] A. Sakai, K. Kuga, and S. Nakatsuji, *J. Phys. Soc. Jpn.* **81**, 083702 (2012).
- [25] K. Matsubayashi, T. Tanaka, A. Sakai, S. Nakatsuji, Y. Kubo, and Y. Uwatoko, *Phys. Rev. Lett.* **109**, 187004 (2012).
- [26] M. Tsujimoto, Y. Matsumoto, T. Tomita, A. Sakai, and S. Nakatsuji, *Phys. Rev. Lett.* **113**, 267001 (2014).
- [27] M. Matsunami, M. Taguchi, A. Chainani, R. Eguchi, M. Oura, A. Sakai, S. Nakatsuji, and S. Shin, *Phys. Rev. B* **84**, 193101 (2011).
- [28] Y. Tokunaga, H. Sakai, S. Kambe, A. Sakai, S. Nakatsuji, and H. Harima, *Phys. Rev. B* **88**, 085124 (2013).
- [29] Y. Shimura, Y. Ohta, T. Sakakibara, A. Sakai, and S. Nakatsuji, *J. Phys. Soc. Jpn.* **82**, 043705 (2013).
- [30] See Supplemental Material, which includes Refs. [33–35], at <http://link.aps.org/supplemental/10.1103/PhysRevB.91.241102> for the experimental method and the analysis of the CEF under magnetic field.
- [31] K. Hattori and H. Tsunetsugu, *J. Phys. Soc. Jpn.* **83**, 034709 (2014).
- [32] S. Nagashima, T. Nishiwaki, A. Otani, M. Sakoda, E. Matsuoka, H. Harima, and H. Sugawara, *JPS Conf. Proc.* **3**, 011019 (2014).
- [33] K. Lea, M. Leask, and W. Wolf, *J. Phys. Chem. Solids* **23**, 1381 (1962).
- [34] K. Araki, Y. Shimura, N. Kase, T. Sakakibara, A. Sakai, and S. Nakatsuji, *JPS Conf. Proc.* **3**, 011093 (2014).
- [35] Y. Aoki, T. Namiki, T. D. Matsuda, K. Abe, H. Sugawara, and H. Sato, *Phys. Rev. B* **65**, 064446 (2002).